Biomaterials Science

PAPER

View Article Online
View Journal | View Issue

Cite this: *Biomater. Sci.*, 2018, **6**, 501

Evaluation of RGD functionalization in hybrid hydrogels as 3D neural stem cell culture systems†

Emanuele Mauri, *[a] Alessandro Sacchetti,[a] Nunzio Vicario,[b] Luca Peruzzotti-Jametti,[b] Filippo Rossi ‡[a] and Stefano Pluchino*‡[b]

Received 15th November 2017,
Accepted 8th January 2018

DOI: 10.1039/c7bm01056g

rsc.li/biomaterials-science

The use of neural stem cells (NSCs) in cell therapy has become a powerful tool used for the treatment of central nervous system diseases, including traumatic brain and spinal cord injuries. However, a significant drawback is related to the limited viability after transplantation *in situ*. The design of three-dimensional (3D) scaffolds that are capable of resembling the architecture and physico-chemical features of an extracellular environment could be a suitable approach to improve cell survival and preserve their cellular active phase over time. In this study, we investigated NSC adhesion and proliferation in hydrogel systems. In particular, we evaluated the effect of RGD binding domains on cell fate within the polymeric scaffold. The introduction of a tripeptide *via* hydrogel chemical functionalization improved the percentage of proliferating cells until 8 days after seeding when compared to the unmodified scaffold. The beneficial effects of this 3D culture system was further evident when compared to a NSC monolayer (2D) culture, resulting in an approximately 40% increase in cells in the active phases at 4 and 8 days, and maintained a difference of 25% until 21 days after seeding.

Introduction

Biomaterial-based therapies represent one of the last and promising approaches to interface with native tissues in predefined ways.[1–3] Many researchers have focused their attention on the design of biocompatible materials able to engage in a dialogue with the biological environment and a wide range of successful systems have been produced for the detection of biological compounds,[4,5] the delivery of drugs or active substances in response to diseases[6–8] and the on-demand presentation of bioactive ligands to direct cell behavior and regenerate tissues.[9,10] In particular, the synergy of the protective and repair measures could be the solution to injuries and disorders. Among them, disruptions to the central nervous system (CNS) are one of the most devastating conditions due to severe and permanent deficits, often resulting in the loss of neuronal cell bodies, axons and associated glia support.[11,12] The physical consequences are commonly visible in traumatic brain injury (TBI) and spinal cord injury (SCI). The limited ability of the CNS to spontaneously regenerate is related to the cell inhibition around the lesion site and to the formation of dense scar tissue that impair the axonal regeneration and the functional recovery of the spinal cord. Among the SCI treatments, the transplantation of certain stem cells into the damaged area is one of the most commonly used regenerative approaches reported over the last few years.[13–15] Especially, neural stem cells (NSCs) are under investigation with regards to their support in axonal regeneration, neuroprotection or resetting the inflammatory response to a mode that heals the damage tissue.[16–18] This type of cell represents a great potential tool, not only because of their capacity to integrate into the host tissue, contributing to the replacement of damaged cells but also because of several bystander capacities, such as tissue trophic support and immune-regulation.[19] Therefore, they are versatile and generally available from different sources, including embryonic, fetal, adult and induced pluripotent stem cells. However, there are some issues in regard the low viability, lack of control on stem cell fate and the reduced cell conjunction with existing neural circuity after transplantation. The crucial aspect of cell survival may be approached using a three-dimensional (3D) substrate, which is able to host cells and create a suitable biomimetic environment where they can proliferate.[20]

As reported in the literature,[21,22] two-dimensional (2D) monolayer cells cultured on a substrate does not adequately

[a]*Department of Chemistry, Materials and Chemical Engineering "Giulio Natta", Politecnico di Milano, via Mancinelli 7, 20131 Milan, Italy.*
E-mail: emanuele.mauri@polimi.it; Fax: +39 022399 3180; Tel: +39 022399 3130
[b]*Department of Clinical Neurosciences - Division of Stem Cell Neurobiology, Wellcome Trust-Medical Research Council Stem Cell Institute and NIHR Biomedical Research Centre, University of Cambridge, Clifford Allbutt Building - Cambridge Biosciences Campus, Hills Road, CB2 0HA Cambridge, UK.*
E-mail: spp24@cam.ac.uk; Fax: +44 (0)1223 331174; Tel: +44 (0)1223 331163
†Electronic supplementary information (ESI) available. See DOI: 10.1039/c7bm01056g
‡These authors share last authorship.

take into account the natural environment of cells when compared to a 3D system, which is more reflective of *in vivo* cellular response. The additional dimensionality of 3D cultures mimics the influence over the spatial organization of the cell surface receptors engaged in the interactions with surrounding cells and also affect the signal transduction from the outside to the inside of cells, influence gene expression and cellular behavior, motility and migration similarly to *in vivo* conditions. Hydrogels are an important class of highly hydrated biomaterials commonly used in drug delivery, regenerative medicine and tissue engineering due to their tunable physico-chemical properties and their 3D structure.[23,24] By complying with the biocompatibility and biodegradability criteria, hydrogels can be produced through smart combinations of natural and synthetic polymers. The natural hydrogels impart biological activity and typically promote cell interaction, and the synthetic polymers offer the opportunity to tailor the scaffold architecture due to their reproducible characteristics such as molecular weight, degradation and mechanical properties. Their swelling behavior allows for the exchange of ions and metabolites with tissue fluids to maintain the biological chemical balance with the surrounding environment and the diffusion of biomolecules preserving hydrogel physical structure.[25,26] In addition, their porous morphology consents the outline of the *in vivo* distribution of metabolites, nutrients, oxygen and signaling molecules. Nowadays, their use as permissive microenvironments to enhance cell survival and control stem cell fate is a significant challenge, in particular in stem cell-based treatments for CNS regeneration.[13,27] The syntheses of hydrogels with an inert surface that prevents the non-specific adsorption of ligands/proteins or with biological molecules covalently incorporated within the scaffold represent two different alternatives to pursue this objective.[28–30] In this work, we have investigated both these strategies. We have proposed the use of two hydrogels composed of polyethylene glycol (PEG), agarose and polyacrylic acid (PAA) as a 3D culture system to preserve the NSC viability over time.

The first hydrogel is a scaffold without polymer conjugation to biomolecules, whereas the second was characterized by PAA functionalization with the cell-adhesive and cell-recognition tripeptide Arg-Gly-Asp (RGD) prepared using a copper-catalyzed azide–alkyne cycloaddition (CuAAC) reaction. In this case, we introduced a stable and uncleavable bond between the polymer and the RGD molecule, in order to preserve the potential effect of the functionalization in the bioenvironment over time. We have monitored the cell behavior and spatial organization within the two scaffolds and compared the obtained results against a 2D NSC culture system. In particular, the NSCs trend towards the quiescent state was recorded and correlated to the cytocompatibility of the biomaterial.

The design of a smart injectable system, such as a hydrogel, appropriately functionalized, conformable to various structures and highly porous may provide suitable conditions to simulate the *in vivo* cellular environment, upgrading the stem cell curative actions *in situ*.

Experimental

Materials

The polymers used in hydrogel synthesis were: PAA (average M_n = 130 kDa, 35% w/w solution in water, Sigma Aldrich Chemie GmbH, Germany), carbomer 974P (MW = 1 MDa, Fagron, The Netherlands), polyethylene glycol (PEG, MW = 2 kDa, Sigma-Aldrich Chemie GmbH, Germany) and agarose (MW = 300 kDa, Invitrogen, ThermoFisher Scientific, USA). Propidium iodide solution was obtained from Invitrogen, ThermoFisher Scientific (USA). Primary antibody rabbit anti-ki67 (Rb ki67) and unconjugated secondary antibody goat anti-rabbit Alexa Fluor 647 were purchased from Abcam (UK). Normal goat serum (NGS) was obtained from Sigma-Aldrich. DMEM/F12 was obtained by Life Technologies (USA). The other chemicals were purchased from Sigma-Aldrich (Germany). The materials were used as received. Solvents were of analytical grade. The RGD derivative was stored at −20 °C. The NMR experiments were carried out on a Bruker AC (400 MHz) spectrometer using chloroform ($CDCl_3$) or deuterium oxide (D_2O) as the solvent and chemical shifts were reported as δ values in parts per million with respect to TMS used as an internal standard. The FT-IR spectra were recorded on a Thermo Nexus 6700 spectrometer coupled to a Thermo Nicolet Continuum microscope equipped with a 15× Reflachromat Cassegrain objective at a resolution of 4 cm^{-1} using the KBr pellet technique. In regard the evaluation of the immunofluorescence of the NPCs loaded within the hydrogel systems, the frozen hydrogel slides with stained NPCs were collected onto SuperfrostPlus slides by Thermo Fisher Scientific (USA).

PAA-RGD functionalization

The chemical modification of PAA with the RGD moiety was accomplished as discussed in our previous work.[31] Briefly, the procedure involved two steps. The first step was the functionalization of PAA with alkyne groups.

PAA (500 mg, 6.94 mmol) was dissolved in distilled water (15 mL) and the following reagents were sequentially added: propargylamine hydrochloride (63.5 mg, 0.69 mmol), a solution of 1-hydroxybenzotriazole hydrate (93.2 mg, 0.69 mmol) in acetonitrile–water (1 : 1, v/v) and ethyldimethylaminopropyl carbodiimide hydrochloride (132.3 mg, 0.69 mmol). After stirring continuously for 24 h, the mixture was dialyzed against an aqueous solution at pH = 5.5 (2000 mL) prepared upon dissolving sodium chloride (11.2 g) in distilled water and the addition of HCl 37% (4 drops). The dialysis was performed for 3 d, with daily changes of the aqueous solution and the addition of HCl. After dialysis, the as-obtained product (propargyl PAA) was frozen at −20 °C and lyophilized.

The second step was related to the CuAAC reaction between propargyl PAA and RGD modified azide. The peptide was synthesized manually using the stepwise solid phase Fmoc method and then linked to the N_3 group. The functionalized polymer (78 mg, 0.072 mmol) was dissolved in distilled water and the RGD azide derivative (25 mg, 0.072 mmol) was added.

The resulting reaction mixture was stirred at 60 °C for 24 h. Subsequently, it was cooled to 25 °C and dialyzed against an aqueous solution at pH 5.5 (as reported in the previous step) for 3 d, with daily changes of the aqueous solution and lyophilized. The as-obtained product was PAA grafting RGD tripeptide through the triazole bond (PAA-RGD).

Hydrogel synthesis

The synthesis of the hydrogel without any chemical functionalization (hereinafter referred to as HG) was performed using a microwave-assisted strategy. Branched polyacrylic acid carbomer 974P (35 mg) was dissolved in a phosphate buffered saline solution (PBS, 5 mL). PEG (300 mg) and glycerol (50 μL) were added to the resulting solution and the mixture was stirred for 30 min and left to settle for 1 h. The pH was adjusted to 7.4 using 1 M NaOH. The resulting solution was used in the 3D network synthesis as follows: agarose (25 mg) was added to the mixture (5 mL) and the system subjected to electromagnetic stimulation (500 W irradiated power) for 30 s and heated to 80 °C to induce the condensation reaction between the carboxyl and hydroxyl groups. The reactor was kept closed to avoid any eventual loss of solvent vapors and finally, the gelling solution was poured in cylinders (0.25 mL of mixture in each cylinder with a diameter of 1.1 cm) upon cooling, until gelation occurred.

Hydrogel-RGD synthesis

Hydrogels with RGD functionalization (labelled as HG-RGD) were prepared starting with the dissolution of carbomer 974P (25 mg) and PAA-RGD (10 mg) in PBS solution (5 mL). Then, PEG (300 mg) and glycerol (50 μl) were added and the system was stirred for 30 min. The resulting solution was left to settle for 1 h. The hydrogels were formed using the microwave-assisted reaction using the procedure described for HG (previous section).

Swelling behavior

To assess the swelling behavior, the hydrogel samples were first immersed in PBS for about 24 h, then freeze-dried, weighed (W_d) and poured into an excess of PBS to achieve complete swelling at 37 °C under a 5% CO_2 atmosphere. The swelling kinetics were measured gravimetrically; the samples were removed from the PBS at regular time points. Then, the hydrogel surfaces were wiped with moistened filter paper in order to remove the excess solution and then weighed (W_t). The swelling ratio (Q_m) was calculated using the following equation:

$$Q_m = \frac{W_t - W_d}{W_d} \times 100 \quad (1)$$

where W_t is the weight of the wet hydrogel as a function of time and W_d is the weight of the dried sample.

Rheology

The rheological analyses of HG and HG-RGD were performed at 37 °C using a Rheometric Scientific ARES instrumentation (TA Instruments, New Castle, DE, US) equipped with 30 mm parallel plates with a 4 mm gap between them. The oscillatory responses (G', elastic modulus and G'', loss/viscous modulus) were determined at low values of strain (0.02%) over the frequency range 0.1–100 rad s^{-1}.[32] Dynamic strain sweep (DSS) tests were also performed at a frequency of 20 rad s^{-1} over the strain range of 0.01–100%. The pseudoplastic behavior was also investigated. The behaviors of shear stress and viscosity as a function of shear rate were examined and the linearity of the viscoelastic properties was verified.

Neural stem cells

NSC lines were prepared from the subventricular zone (SVZ) of 4- to 8-week-old C57/Bl6 female mice, as previously reported.[33,34] Briefly, mice were humanely culled by cervical dislocation followed by decapitation, the parietal bones were cut cranially to caudally using micro-surgery scissors and their brain removed. A brain slice matrix was used to obtain 3 mm thick brain coronal sections starting from 2 mm after the anterior pole of the brain. The SVZ of the lateral ventricles was isolated from the coronal sections using iridectomy scissors. Tissues derived from at least 2 mice were pooled to generate the cultures. The dissected tissues were transferred to a 15 mL tube using digestion medium [balance salt solution (EBSS, Gibco), papain (1 mg mL^{-1}, Worthington), ethylenediaminetetraacetic acid (EDTA) (0.2 mg mL^{-1}, Sigma-Aldrich) and L-cysteine (0.2 mg mL^{-1}, Sigma-Aldrich)] and incubated for 45 min at 37 °C on a rocking platform. At the end of the incubation, the tube was centrifuged at 200 g for 12 min, the supernatant was removed and the pellet was mechanically disaggregated using 2 mL of EBSS. The pellet was centrifuged again at 200 g for 12 min and then dissociated with a 200 μL pipette and seeded in complete growth medium (CGM).

CGM was comprised of mouse NeuroCult™ basal medium (Stem Cell Technologies) and mouse NeuroCult™ proliferation supplements (Stem Cell Technologies) with 2 μg mL^{-1} heparin, 20 ng mL^{-1} EGF and 10 ng mL^{-1} bFGF. After approximately 4–7 d, a small percentage of the isolated cells began to proliferate giving rise to neurospheres. When the neurospheres reached the necessary dimension (150–200 μm diameter), the cells were harvested in a 15 mL tube and centrifuged at 100 g for 8 min. The supernatant was then removed and the pellet dissociated using enzymatic digestion with Accumax™ at 37 °C for 10 min. The number of viable cells was determined by trypan blue exclusion and the viable cells were re-seeded at a clonal density of 8000 cells per cm^2. The NSCs were transduced *in vitro* using a third-generation lentiviral carrier (pRRLsinPPT-hCMV) coding for the enhanced farnesylated (f) GFP, which targets the fluorescent protein to the inner plasma membrane of transduced cells.[35] The functional stability of these cells (in the absence or in the presence of the lentiviral transcript) was confirmed using clonal and population studies.[33] Briefly, the neurospheres were harvested, dissociated to a single cell suspension and seeded at high density [1.5 × 10^6 in a T75 cm^2 flask (Sigma-Aldrich)] in 5 mL of fresh medium. After 12 h, 3 × 10^6 T.U. mL^{-1} of lentiviral vectors were added and 6 h later an additional 5 mL of fresh medium

was added. 72 h after viral transduction, the cells were harvested and re-seeded at normal concentration. The transgene expression was measured using FACS analysis before transplantation and >98% of cells were found to be labelled. Mycoplasma negative NSCs at passage $n \leq 25$ were used in all the experiments.

Cell loading

The NSCs were added directly onto the HG and HG-RGD sponge-like hydrogels.[28] The latter were obtained as lyophilized scaffolds, as follows: after their synthesis, the hydrogels were separately submerged in PBS solution for 2 h, frozen on dry ice for 5 min, transferred at −80 °C overnight and then dried under the following conditions: 0.5 mbar and −40 °C.

The resulting lyophilized gels were sterilized for at least 30 min, each side, *via* UV irradiation before seeding the cells. The NSCs were harvested and suspended at a density of 1.25×10^6 cells per mL in growth medium. A 40 μL aliquot of cells was added directly onto one side of the freeze-dried hydrogel sample and placed in an incubator at 37 °C for 20 min. Subsequently, another 40 μL aliquot was added on the other side of the gel. The hydrogels were left to swell for 30 min in an incubator at 37 °C, then placed in a 24 multi-well cell culture plate and 1 mL of growth medium was added. The loaded samples were stored and monitored in an incubator at 37 °C, replacing the medium every 2 d. Each hydrogel contained approximately 100 000 cells. Cell seeding in the 2D substrate was performed as follows: after placing one round glass coverslip in each well of a 24 multi-well plate, laminin was added to the cell suspension in growth medium (1 : 100) and the resulting cell solution was poured into each glass coverslip (80 μL) and incubated for 30 min at 37 °C. In this way, we replicated the same amount of cells within the hydrogel samples in the 2D experiments. Then, a solution of laminin and growth medium (1 : 100) was added (500 μL) to each well and the resulting systems were stored and monitored in an incubator at 37 °C, replacing the medium every 2 d.

Cellular immunofluorescence *in vitro*

Immunofluorescence on the NSCs *in vitro* was performed as described. The hydrogel medium was replaced with a solution of propidium iodide (PI) 500 nM (1 mL) and the system incubated at 37 °C for 5 min. Then, the samples were rinsed five times using PBS 1× (1 mL) in order to remove any free dye remaining in the solution. The gels were stored in an incubator during each washing step, for 8 min. Finally, they were incubated for other 5 min at 37 °C. The PBS solution was removed and cells were fixed using paraformaldehyde (PFA) solution 4% added to each hydrogel well for 10 min. Each sample was rinsed three times using PBS 1× and then incubated for 2 h at room temperature (r.t.) using a blocking solution (300 mL, comprised of PBS 1×, 0.1% Triton X-100 and 10% normal goat serum) to avoid a-specific binding of the used antibodies during intracellular staining.

The resulting HG and HG-RGD with fixed NSCs were treated with an appropriate primary antibody diluted in PBS 1× (300 mL), overnight at 4 °C. The solution was comprised of PBS 1× with 0.1% Triton X-100, 1% NGS and antibody Rb ki67 (1 : 500). The samples were then washed two times using a solution of 0.1% Triton X-100 in PBS 1× and incubated for 1 h at r.t. with the secondary antibody solution (300 μL) prepared using PBS 1×, 0.1% Triton X-100, 1% NGS and anti-rabbit Alexa Fluor 647 (1 : 1000). Each hydrogel was washed three times with 0.1% Triton X-100 in PBS 1× solution and the NPCs nuclei were stained using 4,6-diamine-2-fenilindole (1 μL mL^{-1}, DAPI) for 3 min. Finally, the samples were washed three times using PBS 1×. The obtained HG and HG-RGD systems were embedded in optimal cutting temperature (OCT) tissue tek compound and snap frozen in dry ice. The frozen blocks were placed in a cryostat (Leica) and 30 μm thick sections were cut and collected onto SuperfrostPlus microscope slides. The latter were then mounted using Fluorescent mounting medium. The samples were examined and photographed using a laser scanning confocal microscope TCS-SP2 (Leica Inc., Wetzlar). In order to analyze the cell distribution throughout the whole gel, six sections of each HG and HG-RGD spaced at 60 μm were acquired at 63× magnification. The immunofluorescence and viability analyses were performed at 1, 4, 8, 14 and 21 d after NSC seeding on the sponge-like gel samples. The immunofluorescence of the laminin samples was performed in the same manner of hydrogels, however, after the last washing step using PBS 1× solution, the round glass coverslips with cells and laminin were directly mounted with Fluorescent mounting medium and evaluated on a confocal microscope.

LDH assay

The determination of the released lactate dehydrogenase (LDH) was performed using a medium of the hydrogels HG, HG-RGD and laminin (conditioned medium) after cell seeding at defined time points (1, 4, 8, 14, 21 d). The collected medium was used as the supernatant for the new NPCs cultures.

After incubation, the resulting systems were collected and then centrifuged at 600 g for 10 min. The supernatant was poured in a 96-well plate (20 μL each well), LDH release reagent (30 μL) was added to mix completely and then incubated at r.t. for 30 min. The cell cytotoxicity was measured using the absorbance (at 490 nm) and the results were compared with that of the control wells to determine the relative cell viability.

Statistical analyses

Statistical analyses were performed using Prism software (Graph-Pad). The applied statistical tests were two-way ANOVA followed by Tukey's *post hoc* test, as reported in the figure legends. The data are presented as the mean ± SEM.

Results and discussion

Hydrogel chemical characterization

The difference between the HG and HG-RGD samples is related to the use of the PAA-RGD component in their synthesis. RGD is the most effective and commonly employed peptide sequence for stimulated cell adhesion on synthetic substrates due to its ability to mimic cell adhesion proteins, bind to cell-surface receptors and its biological impact on cell behavior and survival.[36–38] The design of a stable RGD motif linker to the synthetic surface is the focal point to achieve strong cell adhesion; many researchers have proposed a covalent attachment to the polymer, exploiting functional groups such as hydroxyl, amino or carboxyl groups, which are already available on the surface of the polymer structure or specifically introduced by blending, copolymerization, chemical or physical treatments. In order to avoid any potential bond liability between RGD and PAA, we proposed a click chemistry approach. PAA modification with alkyne moieties and grafting of the RGD to an azide group[31] allowed the formation of triazole through the CuAAC cycloaddition. Triazole is stable in metabolic and chemical degradations[39,40] and uncleavable under physiological conditions. The FT-IR spectrum (ESI, Fig. S1†) shows the characteristic peaks of triazole[41] at 1445 cm^{-1}, whereas the wavenumbers range 3600–2900 cm^{-1} correspond to the stretching vibration of –OH residual groups with a partial overlap with the peak of C–H stretching at 2950–2850 cm^{-1}. The carbonyl stretch C═O was detectable around 1700 cm^{-1}, the PAA $-CH_2$ stretching is visible in the range 1435–1300 cm^{-1} and the signal at 1256 cm^{-1} was representative of C–O vibrations. As reported in our previous work,[31] the functionalization of PAA occurred by modifying only 10% of its carboxyl groups with a triple bond, in order to preserve the residual groups for hydrogel synthesis. In this way, PAA-RGD took part in the formation of the 3D HG-RGD polymeric scaffold and was not physically entrapped within the mesh. This approach allowed the design of an alternative scaffold to HG, which was attributed the potential variations in the NPCs behavior to the grafted RGD.

The HG and HG-RGD hydrogels were produced using the chemical cross-linking between the carbomer (and PAA-RGD in HG-RGD samples), PEG and agarose *via* a microwave-assisted polycondensation reaction. This chemistry is based on the efficient heating of the materials *via* the "microwave dielectric heating" effect and is dependent on the ability of a specific component (solvent or reagent) to absorb microwave energy and convert it into heat.[32,42] Heating to 80 °C leads to higher macromer mobility and thus, enhances the short-range interconnections among the functional groups of the polymers. In details, the carboxyl groups and hydroxyl groups produce local networks which, as the esterification proceeds, give rise to the final three-dimensional macrostructure. Gel formation is progressive and occurs before the sol/gel transition temperature, and is complete within 10 min, which avoids damage to the structures of the components. This peculiar feature allows the hydrogels to complete their gelation directly *in situ*, which are still injectable in the sol state thanks to their thixotropic nature.[31,32] The used polymers are well known as biocompatible materials for therapeutic and tissue engineering approaches, thanks to their anti-inflammatory and clinical properties, and promising interaction with cells.[1,43–45] The building blocks of the macromolecules form a stable structure made up of mostly C–C bonds with ester bonds used as cross-linking points and, in the HG-RGD sample, the presence of the grafted tripeptide. A schematic representation of the two synthetized hydrogels is shown in Fig. 1A.

The formation of ester bonds in HG and HG-RGD is visible in their FT-IR spectra (Fig. 1B), where peaks corresponding to the symmetric (around 1600 cm^{-1}) and asymmetric (around 1400 cm^{-1}) CO_2 stretches are detectable. The two spectra also show the signals related to the C–O–C stretching vibrations (range 900–1000 cm^{-1}) that represent the glycosidic bond between the monosaccharide units (typical of the agarose structure) and ester groups. In the HG-RGD sample, the presence of RGD functionalization was confirmed by its detectable peaks corresponding to the amide I (*, 1670 cm^{-1}, C═O stretching) and amide II (**, 1560 cm^{-1}, N–H bending) bands,[46] in addition to the triazole signal. These considerations show that the synthesis of the gel scaffold was correctly achieved and the discussed tripeptide functionalization was successfully obtained.

Hydrogel physical characterization

Hydrogels are polymeric scaffolds able to link and retain a large amount of water, which gives them the advantage over other matrices by mimicking the aqueous environment of the extracellular matrix (ECM).[47] During the swelling of a hydrogel network, the polymer chains assume a stretched conformation, counterbalanced by an elastic force acting in the opposite direction generated by increasing the elongation of the system and this force limits the stretching process. On the other hand, polymer swelling is promoted by the polymer-solvent mixing process, which lowers the total free energy by increasing the system's entropy. The action of these opposite forces leads to the attainment of a thermodynamic equilibrium. The experimental results obtained from the HG and HG-RGD samples show that both the samples exhibited fast swelling kinetics and their swelling equilibrium was reached within 30 min. In particular, Fig. 1C highlights the similar swelling trends observed for HG (in red) and HG-RGD (in black); HG reached a swelling ratio equal to 1100% and HG-RGD was characterized by a value of about 1350%. As reported in previous work,[23,31,48] the swelling phenomenon exhibits a high dependence on the solute loaded within the polymeric network. In this case this dependence was present, but less visible, because the RGD peptide was integrated with the polymeric network and does not create a high hindrance to the gelation process. This suggests that the PAA chemical modification did not significantly affect the physical properties of the network, despite the functionalization in HG-RGD decreasing the number of reactive sites with a consequent decrease in the cross-linking density. Furthermore, as pre-

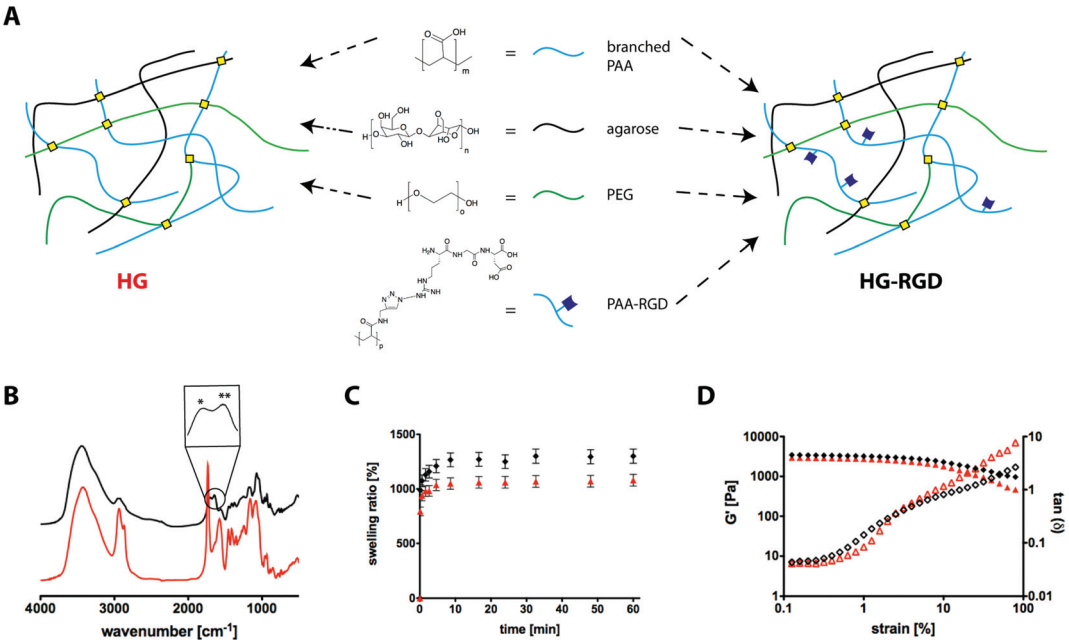

Fig. 1 Physico-chemical characterization of the hydrogels. A: Schematic representation of the unmodified (HG) and RGD-functionalized (HG-RGD) hydrogels. B: FT-IR spectra of HG (red) and HG-RGD (black); the RGD amide I (*) and II (**) signals are emphasized in the HG-RGD spectrum. C: Swelling kinetics of HG (▲, red) and HG-RGD (▲, black); the equilibrium was reached in the first 30 min and maintained over time. D: Rheological behavior of HG (G'▲ red, tan(δ) Δ red) and HG-RGD (G'♦ black, tan(δ) ◊ black) hydrogels.

viously demonstrated,[49] the gels swelling kinetics were much faster than their degradation. In regard the rheology (Fig. 1D), for both samples the storage modulus (G') was found to be approximately one order of magnitude higher than the loss modulus (G''), indicating an elastic rather than viscous material. Both moduli were also essentially independent of frequency.

In detail, G' values observed for HG and HG-RGD were 3000 Pa and 3500 Pa, respectively. The RGD modified material presented stiffer and more elastic properties than HG, which can be attributed to the interactions between the polymeric network and RGD pendant groups. Also, in this case, the influence of RGD does not irreversibly change the rheological properties due to the integration of the polymer chains and the absence of high steric hindrance. The DSS tests showed that the behaviour of both HG and HG-RGD is dominated by the elastic modulus at low strain values. Increasing the strain values, the elastic structure of the network breaks down and the elastic modulus rapidly decreases. The crossover strain (γ_c) can be evaluated as the value at which the contribution of the material damping tan(δ) is predominant with respect to G'. At low values of strain, the two G' trends indicate the presence of a closely-packed polymeric network and the behaviors of tan(δ) are very similar, thus indicating very similar, liquid-like behavior. Our previous work has also revealed that dried hydrogels possess a highly entangled structure.[31] There are some larger pores containing small pores and some fibrillar networks on the pore walls. In addition, most of the pores are interconnected, giving rise to a porous structure with a complex 3D network.

Hydrogel effect on the NSC viability *in vitro*

We tested the impact of a 3D structure on NSCs, compared to a NSC monolayer system (2D), on laminin. We also investigated how the presence of the RGD motifs could improve cell adhesion and viability. As reported in the literature,[21,50,51] the 3D cell culture system represents the microenvironment more accurately, where the cells reside in the tissues and provide more predictive data for *in vivo* experiments. The same amount of NSCs was seeded over the 2D substrate and within the hydrogels and monitored after 1, 4, 8, 14 and 21 d in order to study cellular behavior over time. Propidium iodide was used to detect the dead cells and its staining protocol was applied before NSC fixation using PFA, whereas ki67 was chosen as a marker for cells in the non-quiescent state, including those in the proliferating active phase. It was conjugated to a secondary antibody with different absorption/emission spectra than the PI, GFP membrane and DAPI nuclear staining, avoiding overlaps in the confocal images recorded.

Fig. 2 shows the NSC spatial organization and proliferation on laminin (Fig. 2Aa, Bb, Cc, Dd and Ee) and within the HG (Fig. 2Ff, Gg, Hh, Ii and Jj) and HG-RGD (Fig. 2Kk, Ll, Mm, Nn and Oo) networks, at the indicated time points.

The seeded cells over the 2D substrate were able to proliferate and rapidly grow achieving a condition close to confluence at day 8. The high increment of cell population progressively reduced the number of NSCs in the non-quiescent state, which can be qualitatively observed in the decrease in the number of ki67 positive cells (Fig. 2a–e). In both the hydrogel systems, the NSCs were able to adhere to the polymer chains and pro-

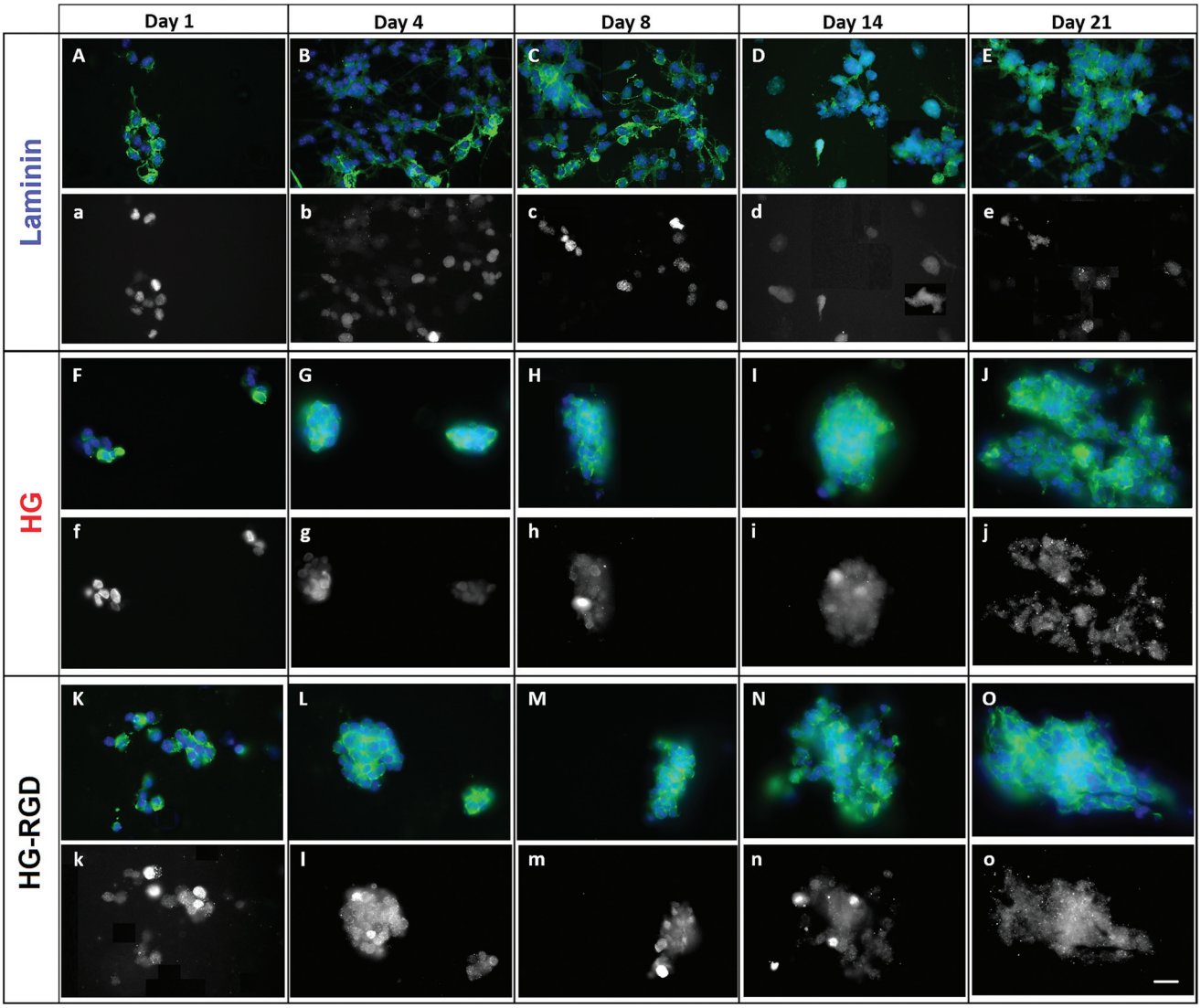

Fig. 2 Confocal representative images (63×) of the NSCs stained with DAPI and GFP (upper case letters, DAPI in blue and GFP in green) and stained with ki67 (lower case letters, ki67 in white) in the laminin (Aa, Bb, Cc, Dd, Ee), HG (Ff, Gg, Hh, Ii, Jj) and HG-RGD (Kk, Ll, Mm, Nn, Oo) samples. Images were recorded at different time points (1, 4, 8, 14 and 21 d after cell seeding) and were related to 30 μm thick sections for HG and HG-RGD and from a glass coverslip in the laminin samples. The scale bar represents 30 μm.

liferate, giving rise to neurosphere generation. The fraction of ki67 positive NSCs (cells in active phases cellular cycle) in HG and HG-RGD is reported in Fig. 3 and compared to the results obtained on the laminin substrate, over time.

Significantly different trends can be observed in the 3D substrates against laminin. One day after seeding, the percentage of NSCs expressing ki67 was 71% in the 2D system, 74% in the HG sample and slightly above (78%) in the hydrogel with RGD. At day 4, a significant reduction in the non-quiescent cells characterized the laminin monolayer (only 43% of NPCs were stained with the antibody), whereas HG showed that 78% of cells were in the active phase and in HG-RGD up to 87% was observed.

At day 8, the fraction of NSCs expressing ki67 was further reduced to 31% in laminin seeding and was found to be 63% in HG and 71% in HG-RGD.

Monitoring at 14 and 21 days after the seeding, the non-quiescent NSCs decreased in each sample to 24% in laminin substrate, 42% in HG and 50% in HG-RGD. Accordingly, the fraction of dead cells in the 2D configuration increased over time; the NSCs labelled PI achieved values of 22% after 8 days and 60% after 21 days. However, in the HG and HG-RGD networks, the corresponding percentages were around 2% until 8 days and only 6% in HG and 9% in RGD modified scaffold at 21 days (ESI, Fig. S2†). These considerations suggest that use of a 3D polymeric tool appears as a promising NSC culture system to give an opportunity to cells to migrate and proliferate for a longer time than in the 2D culture. Therefore, we have proposed a biocompatible and non-toxic system (ESI, Fig. S3†), which is able to provide an increased superficial area where cells can adhere and grow without spatial restrictions due to

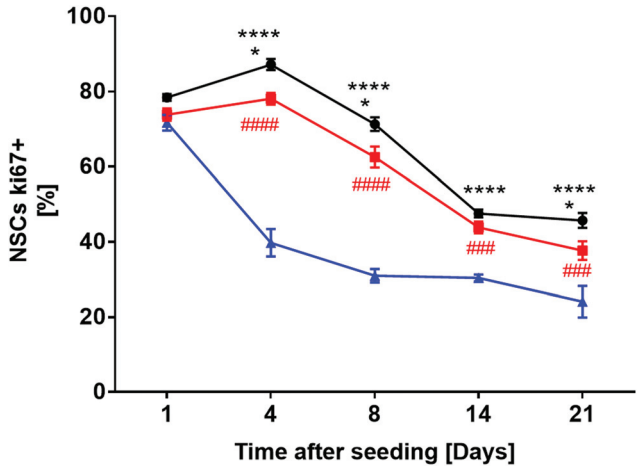

Fig. 3 Graph representing the ki67 positive NSCs trends in the laminin (Δ, blue), HG (□, red) and HG-RGD (○, black) samples, over time. Statistical analysis: two-way ANOVA followed by Tukey's *post hoc* test. Mean ± SEM is reported; n = 6 per group; (*) $p < 0.05$ *vs*. HG, (****) $p < 0.0001$ *vs*. laminin; ($^{###}$) $p < 0.001$ *vs*. laminin, ($^{####}$) $p < 0.0001$ *vs*. laminin.

the hydrogel mesh size and swelling behavior mimicking the natural environment. Furthermore, focusing on comparing the ki67 positive NSCs trends in the unmodified and RGD-functionalized hydrogels, some differences could be recorded. In particular, at day 4 and day 8, the HG-RGD sample was characterized by more proliferating cells than HG (Fig. 3). The bioactivity of the hydrogel was improved due to the presence of bioactive molecules, such as RGD, which is generally detectable in native ECM. After seeding, the effect of the tripeptide, in addition to supporting cell adhesion, to improve the design of a hospitable 3D environment resembling the natural environment of the NSCs, was more than HG system. Another contribution could be related to stiffness. From Fig. 1D it is visible that the storage modulus of HG-RGD was higher than HG. In this direction, several studies have already proven the role of hydrogel elasticity in 3D cell culture systems.[52,53] The influence of the RGD motif was very visible at day 4 and day 8, whereas it became restricted over time (in particular at day 14, where the difference in proliferating NSCs between HG and HG-RGD was about 2%).

This aspect can be explained by considering the continuous increase in the cell population in the 3D scaffolds. The LDH tests (Fig. 4) show the cytotoxicity of the medium surrounding the cells in each sample, which is directly related to the lack of nutrients and all other fundamental constituents in the cell medium.

By taking the media conditioned by each sample and using it as cell culture media for new NSCs, we observed that the release of LDH was prominent for the cells treated with the 14th and 21st day HG and HG-RGD media. This suggests that the conditioned media at the indicated time points were poor of nutrients and the latter were completely absorbed by the NSCs grafted onto the hydrogel network; the high proliferation of cells over time quickly leads to the consumption of the medium components and gave rise to a condition where the beneficial effects of RGD became limited in the corresponding hydrogel system.

On the other hand, conditioned media at 1st and 4th day related to the gel scaffolds seemed to be suitable for supporting the cell cultures. In the laminin samples, the release of LDH was significantly high at 4 days after NSC seeding. Referring to the different NSC behavior and proliferation trends in the 2D and 3D culture systems, the release of LDH reached maximal values earlier in laminin than in HG and HG-RGD, and this trend was maintained over time. Moreover, in the HG-RGD sample, the recorded absorbance values were lower than in HG at day 1 and day 4. These results confirmed that the design of the 3D culture systems allowed an improvement in the cell viability and healthy state with respect to the 2D configuration.

Conclusions

In this work, we have proposed the synthesis of hydrogels as sustainable 3D culture systems able to preserve NSC viability

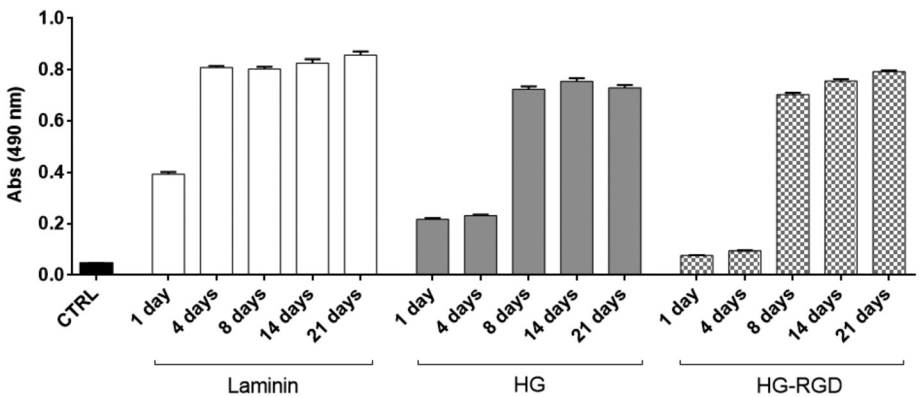

Fig. 4 LDH assay performed for the NSCs treated with conditioned media on the laminin, HG and HG-RGD culture systems at different time points. CTRL represents the LDH release of NSCs in standard growth medium.

and proliferation for longer times than a monolayer configuration. The materials were completely biocompatible and the introduction of the RGD motif produced beneficial results on cell healthy state until 8 days after seeding, allowing a higher number of non-quiescent cells than the corresponding hydrogel without tripeptide modification. In conclusion, the RGD-functionalized hydrogels are an optimized scaffold used to maintain more suitable biological conditions for neural stem cells and can be considered as a candidate to grow, store and preserve NSCs *via* a 3D cell culture approach.

Conflicts of interest

There are no conflicts to declare.

Acknowledgements

The authors would like to thank Dr Simonetta Papa, Dr Pietro Veglianese and Stefano Rimondo for their fruitful discussions. This work was supported by a core support grant from the Wellcome Trust and Medical Research Council to the Wellcome Trust – MRC Cambridge Stem Cell Institute. LPJ was supported by a research training fellowship from the Wellcome Trust (RRZA/057 RG79423).

References

1 Y.-H. Tsou, J. Khoneisser, P.-C. Huang and X. Xu, *Bioact. Mater.*, 2016, **1**, 39–55.
2 Y. Tabata, *J. R. Soc., Interface*, 2009, **6**, S311–S324.
3 L. Li, Z.-Y. He, X.-W. Wei and Y.-Q. Wei, *Regener. Biomater.*, 2016, **3**, 99–105.
4 M. Muskovich and C. J. Bettinger, *Adv. Healthcare Mater.*, 2012, **1**, 248–266.
5 T. Zako and M. Maeda, *Biomater. Sci.*, 2014, **2**, 951–955.
6 E. Mauri, P. Veglianese, S. Papa, A. Mariani, M. De Paola, R. Rigamonti, G. M. F. Chincarini, I. Vismara, S. Rimondo, A. Sacchetti and F. Rossi, *RSC Adv.*, 2017, **7**, 30345–30356.
7 E. Mauri, F. Rossi and A. Sacchetti, *Mater. Sci. Eng., C*, 2016, **61**, 851–857.
8 M. Mekhail, G. Almazan and M. Tabrizian, *Biomater. Sci.*, 2015, **3**, 279–287.
9 M. Bongio, J. J. J. P. van den Beucken, M. R. Nejadnik, S. C. G. Leeuwenburgh, L. A. Kinard, F. K. Kasper, A. G. Mikos and J. A. Jansen, *Eur. Cells Mater.*, 2011, **22**, 359–376.
10 C. Cha, W. B. Liechty, A. Khademhosseini and N. A. Peppas, *ACS Nano*, 2012, **6**, 9353–9358.
11 J. C. DiNunzio and R. O. Williams, *Drug Dev. Ind. Pharm.*, 2008, **34**, 1141–1167.
12 P. J. Horner and F. H. Gage, *Nature*, 2000, **407**, 963–970.
13 R. C. Assuncao-Silva, E. D. Gomes, N. Sousa, N. A. Silva and A. J. Salgado, *Stem Cells Int.*, 2015, 948040, DOI: 10.1155/2015/948040.
14 P. Lu, L. L. Jones, E. Y. Snyder and M. H. Tuszynski, *Exp. Neurol.*, 2003, **181**, 115–129.
15 B. Sandner, P. Prang, A. Blesch and N. Weidner, *Stem Cells Biol. Reg.*, 2015, 155–174, DOI: 10.1007/978-1-4939-1908-6_9.
16 G. Martino, S. Pluchino, L. Bonfanti and M. Schwartz, *Physiol. Rev.*, 2011, **91**, 1281–1304.
17 C. Cossetti, C. Alfaro-Cervello, M. Donega, G. Tyzack and S. Pluchino, *Cell Tissue Res.*, 2012, **349**, 321–329.
18 S. Pluchino, L. Zanotti, M. Deleidi and G. Martino, *Brain Res. Rev.*, 2005, **48**, 211–219.
19 E. Giusto, M. Donega, C. Cossetti and S. Pluchino, *Exp. Neurol.*, 2014, **260**, 19–32.
20 I. Elliott Donaghue, C. H. Tator and M. S. Shoichet, *Biomater. Sci.*, 2015, **3**, 65–72.
21 R. Edmondson, J. J. Broglie, A. F. Adcock and L. J. Yang, *Assay Drug Dev. Technol.*, 2014, **12**, 207–218.
22 S. Knowlton, Y. K. Cho, X. J. Li, A. Khademhosseini and S. Tasoglu, *Biomater. Sci.*, 2016, **4**, 768–784.
23 F. Rossi, G. Perale, G. Storti and M. Masi, *J. Appl. Polym. Sci.*, 2012, **123**, 2211–2221.
24 L. Beria, T. N. Gevrek, A. Erdog, R. Sanyal, D. Pasini and A. Sanyal, *Biomater. Sci.*, 2014, **2**, 67–75.
25 F. Ullah, M. B. H. Othman, F. Javed, Z. Ahmad and H. M. Akil, *Mater. Sci. Eng., C*, 2015, **57**, 414–433.
26 Y. S. Zhang and A. Khademhosseini, *Science*, 2017, **356**, eaaf3627.
27 X. W. Li, E. Katsanevakis, X. Y. Liu, N. Zhang and X. J. Wen, *Prog. Polym. Sci.*, 2012, **37**, 1105–1129.
28 I. Caron, F. Rossi, S. Papa, R. Aloe, M. Sculco, E. Mauri, A. Sacchetti, E. Erba, N. Panini, V. Parazzi, M. Barilani, G. Forloni, G. Perale, L. Lazzari and P. Veglianese, *Biomaterials*, 2016, **75**, 135–147.
29 R. R. Yang, C. X. Xu, T. Wang, Y. Q. Wang, J. N. Wang, D. P. Quan and D. Y. B. Deng, *RSC Adv.*, 2017, **7**, 41098–41104.
30 P. Naghdi, T. Tiraihi, F. Ganji, S. Darabi, T. Taheri and H. Kazemi, *J. Tissue Eng. Regener. Med.*, 2016, **10**, 199–208.
31 A. Sacchetti, E. Mauri, M. Sani, M. Masi and F. Rossi, *Tetrahedron Lett.*, 2014, **55**, 6817–6820.
32 F. Rossi, R. Ferrari, S. Papa, D. Moscatelli, T. Casalini, G. Forloni, G. Perale and P. Veglianese, *Colloids Surf., B*, 2013, **108**, 169–177.
33 S. Pluchino, A. Quattrini, E. Brambilla, A. Gritti, G. Salani, G. Dina, R. Galli, U. Del Carro, S. Amadio, A. Bergami, R. Furlan, G. Comi, A. L. Vescovi and G. Martino, *Nature*, 2003, **422**, 688–694.
34 M. Cusimano, D. Biziato, E. Brambilla, M. Donega, C. Alfaro-Cervello, S. Snider, G. Salani, F. Pucci, G. Comi, J. M. Garcia-Verdugo, M. De Palma, G. Martino and S. Pluchino, *Brain*, 2012, **135**, 447–460.
35 A. Follenzi, L. E. Ailles, S. Bakovic, M. Geuna and L. Naldini, *Nat. Genet.*, 2000, **25**, 217–222.
36 U. Hersel, C. Dahmen and H. Kessler, *Biomaterials*, 2003, **24**, 4385–4415.

37 A. Lagunas, J. Comelles, E. Martínez, E. Prats-Alfonso, G. A. Acosta, F. Albericio and J. Samitier, *Nanomedicine*, 2012, **8**, 432–439.
38 A. C. de Luca, A. Faroni, S. Downes and G. Terenghi, *J. Tissue Eng. Regener. Med.*, 2016, **10**, 647–655.
39 M. Taddei, S. Ferrini, L. Giannotti, M. Corsi, F. Manetti, G. Giannini, L. Vesci, F. M. Milazzo, D. Alloatti, M. B. Guglielmi, M. Castorina, M. L. Cervoni, M. Barbarino, R. Fodera, V. Carollo, C. Pisano, S. Armaroli and W. Cabri, *J. Med. Chem.*, 2014, **57**, 2258–2274.
40 N. Ma, Y. Wang, B. X. Zhao, W. C. Ye and S. Jiang, *Drug Des., Dev. Ther.*, 2015, **9**, 1585–1599.
41 H. B. Li, Q. L. Zheng and C. P. Han, *Analyst*, 2010, **135**, 1360–1364.
42 C. O. Kappe, *Angew. Chem., Int. Ed.*, 2004, **43**, 6250–6284.
43 E. Varoni, M. Tschon, B. Palazzo, P. Nitti, L. Martini and L. Rimondini, *Connect. Tissue Res.*, 2012, **53**, 548–554.
44 M. Xu, J. Q. Zhu, F. F. Wang, Y. J. Xiong, Y. K. Wu, Q. Q. Wang, J. Weng, Z. H. Zhang, W. Chen and S. J. Liu, *ACS Nano*, 2016, **10**, 3267–3281.
45 T. Gros, J. S. Sakamoto, A. Blesch, L. A. Havton and M. H. Tuszynski, *Biomaterials*, 2010, **31**, 6719–6729.
46 J. M. Zhu, C. Tang, K. Kottke-Marchant and R. E. Marchant, *Bioconjugate Chem.*, 2009, **20**, 333–339.
47 A. P. Pego, S. Kubinova, D. Cizkova, I. Vanicky, F. M. Mar, M. M. Sousa and E. Sykova, *J. Cell. Mol. Med.*, 2012, **16**, 2564–2582.
48 G. Perale, F. Rossi, M. Santoro, M. Peviani, S. Papa, D. Llupi, P. Torriani, E. Micotti, S. Previdi, L. Cervo, E. Sundstrom, A. R. Boccaccini, M. Masi, G. Forloni and P. Veglianese, *J. Controlled Release*, 2012, **159**, 271–280.
49 M. Santoro, P. Marchetti, F. Rossi, G. Perale, F. Castiglione, A. Mele and M. Masi, *J. Phys. Chem. B*, 2011, **115**, 2503–2510.
50 E. Knight and S. Przyborski, *J. Anat.*, 2015, **227**, 746–756.
51 J. Vanderburgh, J. A. Sterling and S. A. Guelcher, *Ann. Biomed. Eng.*, 2017, **45**, 164–179.
52 A. J. Engler, S. Sen, H. L. Sweeney and D. E. Discher, *Cell*, 2006, **126**, 677–689.
53 W. J. Hadden, J. L. Young, A. W. Holle, M. L. McFetridge, D. Y. Kim, P. Wijesinghe, H. Taylor-Weiner, J. H. Wen, A. R. Lee, K. Bieback, B.-N. Vo, D. D. Sampson, B. F. Kennedy, J. P. Spatz, A. J. Engler and Y. S. Choi, *Proc. Natl. Acad. Sci. U. S. A.*, 2017, **114**, 5647–5652.

